A Study On Fatigue Resistance And Structural Integrity In Web-Core Composite Bridge Deck Panels

Karpenko, O.; Peeters, T.; Gommers, E.; White, T.; Tromp, L.; Pavlović, M.

Publication date
2024

Document Version
Final published version

Published in
Proceedings of the 21st European Conference on Composite Materials

A STUDY ON FATIGUE RESISTANCE AND STRUCTURAL INTEGRITY IN WEB-CORE COMPOSITE BRIDGE DECK PANELS

O. Karpenko[1], T.Peeters[2], E. Gommers[3], T. White[4], L. Tromp[5], M. Pavlović[6]

[1]Delft University of Technology, Stevinweg 1, 2628CN Delft, The Netherlands,
Email: o.karpenko@tudelft.nl, Web Page: https://www.tudelft.nl/staff/o.karpenko/
[2]Delft University of Technology, Stevinweg 1, 2628CN Delft, The Netherlands,
Email: t.peeters-1@tudelft.nl
[3]Delft University of Technology, Stevinweg 1, 2628CN Delft, The Netherlands,
Email: e.s.gommers@student.tudelft.nl
[4]Delft University of Technology, Stevinweg 1, 2628CN Delft, The Netherlands,
Email: t.j.white@student.tudelft.nl
[5]Royal HaskoningDHV, Rotterdam, The Netherlands.
Email: liesbeth.tromp@rhdhv.com
[6]Delft University of Technology, Stevinweg 1, 2628CN Delft, The Netherlands,
Email: m.pavlovic@tudelft.nl, Web Page: https://www.tudelft.nl/staff/m.pavlovic/

Keywords: GFRP, Web-to-Flange Junctions, fatigue, experiments

Abstract
The presented research aims to examine local fatigue failure modes of Glass Fiber-polymer Composite (a.k.a. GFRP), particularly how the bending of the Web-to-Flange Junctions (WFJ) and tensile loading of the material affects the composite's fatigue resistance. By conducting experimental analyses, the study investigates GFRP's efficacy both as a material and as a component element, drawing parallels with Eurocode standards for steel and concrete.
The coupon tests under static and fatigue loading conditions provided an empirical data on the Ultimate Limit State (ULS) and fatigue resistance of the GFRP composites, including a better understanding of the effects of variation in the facing's thicknesses in the web-core composite on the fatigue response. Subsequent three-point bending tests on the WFJ provided the insights into the strength of WFJ with the first indications on the governing failure mechanisms in the WFJ.

1. Introduction

For civil engineering applications, the renovation of existing bridges and the design of new structures demand innovative and sustainable materials. Glass Fiber-reinforced Polymer (GFRP) composites have emerged as a leading material in this transformation due to their durability, corrosion resistance, and lightweight properties, which are particularly advantageous for bridge construction [1]. GFRP composites represent a promising alternative to traditional materials like timber, steel, and concrete, which are susceptible to deterioration and corrosion over time [2]. The lighter weight of GFRP not only reduces installation costs but also minimizes the load on foundation structures. By replacing old bridges with GFRP structures, municipalities can achieve substantial improvements in durability and a reduction in maintenance costs [3].
Despite these benefits, the integration of GFRP into existing design frameworks like the Eurocode [4]for composite structures introduces complexities. The specificity required in the design guidelines can lead to increased construction costs and project delays. As noted by authors in [5], current design recommendations do not fully accommodate the unique properties of GFRP, necessitating additional research and modification of design codes to enhance their applicability to GFRP-based structures.
Focusing on the structural design innovations, this study examines the material and component properties of web-core panels in GFRP bridge decks. These panels employ unidirectional (UD) fabrics

on the facings to address bending and mitigate local buckling, while incorporating multidirectional laminates in the webs for effective shear transfer. For the continuous connections between the flanges and webs, components known as Web-to-Flange Junctions (WFJs) are constructed using 'wrap-layers', GFRP fabrics wrapped around foam blocks during production to form the outer layers of the webs and inner layers of the facings. To facilitate the design verification of WFJ components, more comprehensive information is required regarding their fatigue behavior. Currently, the existing design codes lack Stress-life (S-N) curves specifically tailored for WFJ components. Conducting fatigue tests on these components can provide the necessary data to establish an S-N curve, thereby aiding in the design process.

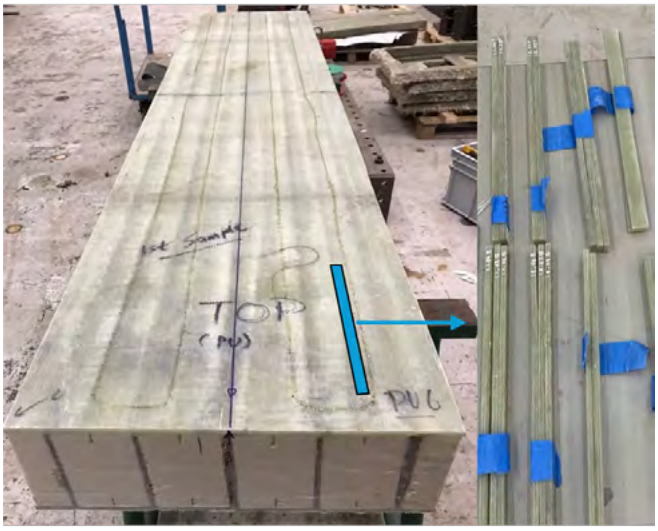

Figure 1. Coupons cut out from the sandwich panel.

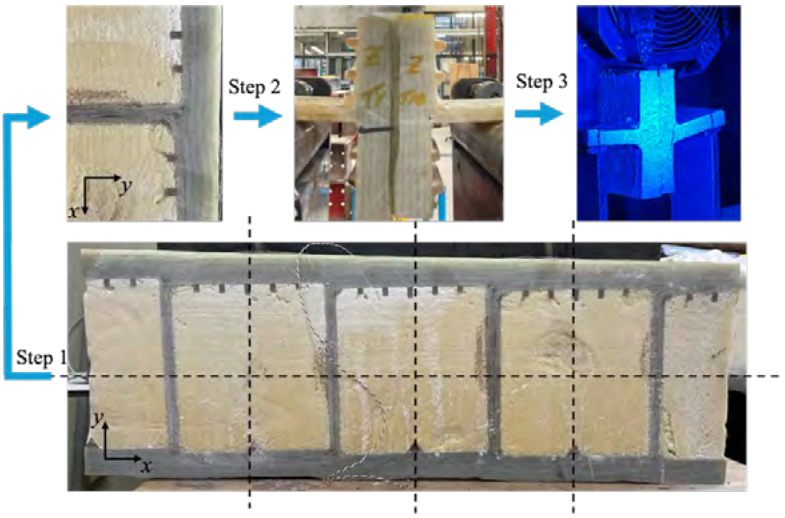

Figure 2. Extraction of web-facing junctions from the sandwich panel.

2. Materials and experimental methods

The coupons and the components (WFJs) are cut out of the GFRP bridge decks, as shown in Figure 1 and Figure 2. The bridge deck is manufactured with vacuum-infused GFRP panels and polyurethane resin that has a core of polyurethane (PU) foam. The deck laminate consists of a Z-shaped layering approach and integrates three types of fibre fabrics. Surrounding the foam blocks are layers of E-glass fabric angled at [+/-45 degrees]. Along the length, three layers of UD E-glass fabrics are laid, with overlaps of two blocks at the top and bottom. The Z-shaped configuration also includes two additional

layers of E-glass fabric oriented at [0/90 degrees] that overlap by 2.5 blocks. Facings have a higher volume fraction of the fibres compared to the webs, due to the production process. The top and the bottom facing of the deck have the lay-up of $[((0/90)_2/0_3)_4/0/90/\pm 45]$ and the web - $[\pm 45_2/(0/90)_2/\pm 45_2]$. The material properties of the composite plies can be found in [6].

2.1. Material tests on coupons

The coupons are cut out from the top and bottom facings of the sandwich panels of the deck as shown in Figure 1. The coupons are extracted from a scaled deck by a factor of 0.5 and the thickness of the coupon specimens is twice as low compared to the thickness of the tests on the WFJs.

The samples are precisely cut using a water jet technique with the dimensions of the coupon specimens to comply with ISO 527 – 4 standard [7] as shown in Figure 3. Owing to the Z-shape layup method used in the decks' production, specimen thicknesses ranged between 9 and 12 mm. The variance in coupon thickness introduces complications in the testing process, requiring the adjustments of modified testing techniques. These complications primarily occur in the gripping area of the testing apparatus, where the specimen's variable thickness causes uneven stress distribution due to a non-uniform clamping surface. Such stress concentrations can induce premature failure of the specimens at the clamping points, thereby complicating the assessment of material properties. Figure 4a highlights the thickness differences in the specimen cross-section A-A. To overcome the thickness transition issues, a mould is designed from timber, shown in Figure 4b. The specific purpose of this mould is to apply a two-component epoxy system [8] at the clamping points to have a flat surface to clamp the specimen in. This resin is fast curing and reaches its full strength in 3 days, after which it is strong enough to resist the high clamping force of the hydraulic wedge grips. Before the specimens are placed in the mould, surface preparation is performed on the regions near the clamps to prevent slipping between the resin and the specimens during testing.

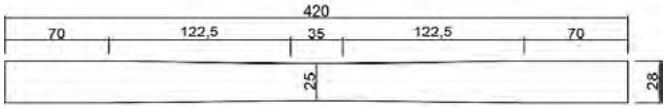

Figure 3. Coupon specimen dimensions.

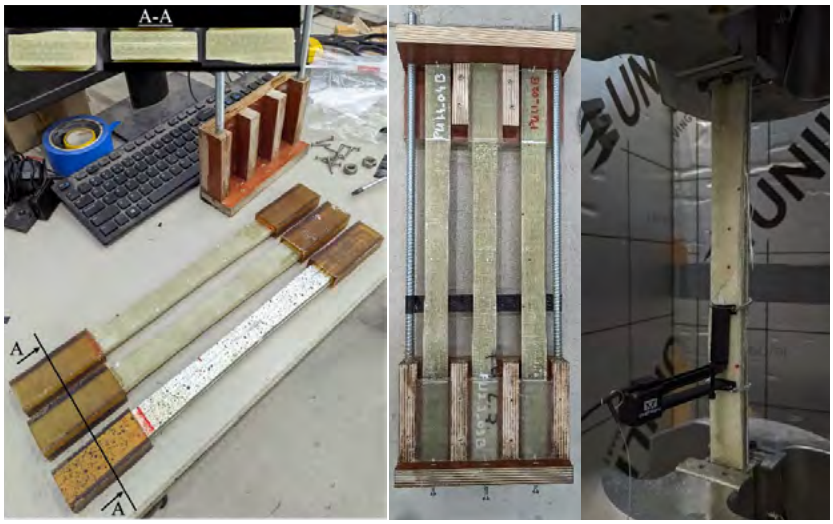

a) Specimen preparation b) Mould design c) Test set-up

Figure 4. Material coupon tests.

Static and fatigue tests are performed on a universal testing machine with a 100kN load cell. The test set-up is shown in Figure 4c. Each static test is subjected to a uniform loading rate of 1 mm/min until the point of failure. The tensile-tensile fatigue tests are performed under the loading ratio of 0.1

considering the three loads of 52%, 37% and 22% of the ultimate load capacity. For every load level a total of 3 successful tests are required, slipped specimens or specimens failing in the clamps are disregarded. The sinusoidal constant amplitude is utilized with frequencies of 2 to 6 Hz, depending on the load levels. During the fatigue tests, an extensometer is used with a gauge length of 50 mm, as shown in Figure 4c.

2.2. Component tests

The bridge deck's web-core sandwich panel contains WFJs, referred to as components, which are shown in Figure 2. The preparation process for these components involves several key steps: 1) Cutting the GFRP panels both in the XZ plane and through the thickness in the YZ plane, specifically between the web sections; 2) Removing the PU foam and using a structural adhesive quick set epoxy to bond the web-facing components together. Steel tabs 25x6x80 mm^3 are also glued in areas designated for load and supports; 3) Applying a thin layer of white, non-reflective paint on one side of the specimens, followed by a random black pattern using a spray gun. This is crucial for detecting crack initiation with the Digital Image Correlation (DIC) system.

Figure 5a shows the specimens' average dimensions, including a width of 50.02±0.53 mm, flange length and thickness ($L_f = 140 \pm 9.16$mm, $t_f = 26.22 \pm 2.25$mm), and web length and thickness ($L_w = 72.45 \pm 3.65$mm, $t_w = 12.86 \pm 2.16$mm).

For testing, a universal testing machine equipped with a 15kN load cell and a total span of 175 mm is used (see Figure 5b). A DIC system featuring a 50.6 MPa camera and polarized blue LED lights captures full-field displacements on the specimens' side surfaces during tests, synchronizing photos with load and displacement data.

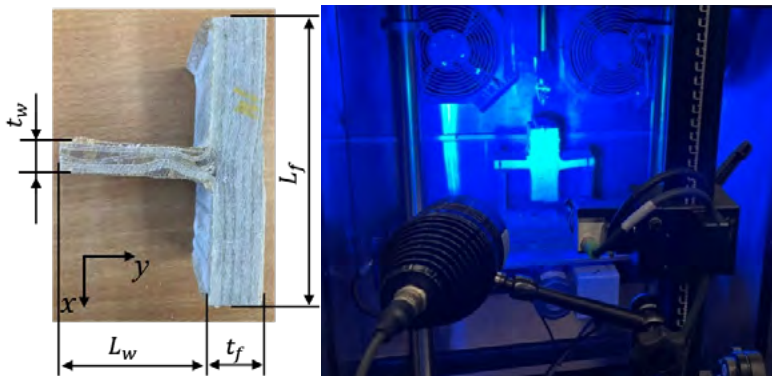

a) Specimen dimensions b) Test set up.

Figure 5. Component tests.

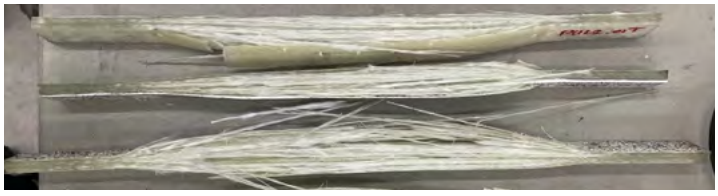

Figure 6. Delamination and fibre failure. Static material tests.

3. Results and discussion

3.1. Material coupon tests

Prior to fatigue tests, static tests are conducted on a set of three specimens to determine the failure loads and stresses. The failure modes are visually inspected, which included delamination and fibre breakage, and consistent across all tests and are shown in Figure 6. The analysis of the specimens is detailed in Figure 7, where the average failure load, displacement and stress are F_{max}=137.68kN, $w_{max} = 11.89$mm and $\sigma_{max} = 577.75$MPa, respectively. The tensile stress is calculated by dividing the applied

load by the initial cross-sectional area at the failure region of the specimen. All three tests show a linear relationship between the applied load and displacement.
Figure 8 illustrates the fatigue response of the tested coupons. Each load level is evaluated with three specimens, resulting in a total of nine tests. The analysis of the material's fatigue performance is carried out in accordance with ASTM E739-10 [9] standards, which involves establishing the S-N relationship through linear regression. The S-N relationship is presented in the following format:

$$\log N = A + B(\log \sigma) \quad (1)$$

where σ is the maximum cyclic stress; N is the number of cycles to failure; A and B are the fitting parameters.
The plot in Figure 8 includes data points, a solid black line representing the logarithmic fit to the data, and dashed black lines are representing the 95% confidence bands for the fit. The fit equation is indicated in Figure 8.

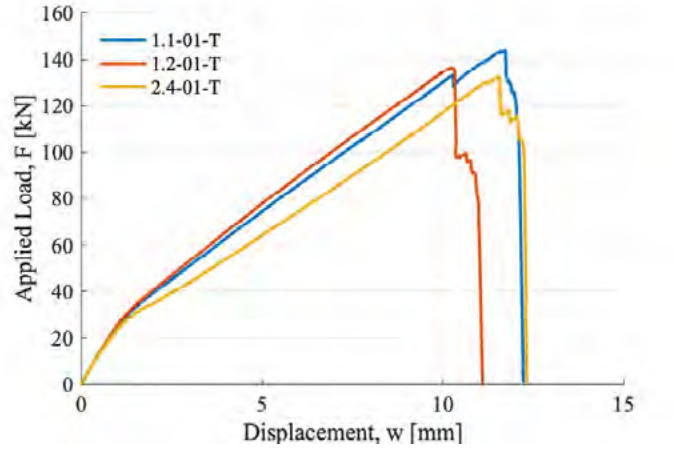

Figure 7. Load-Displacement curves. Static material tests.

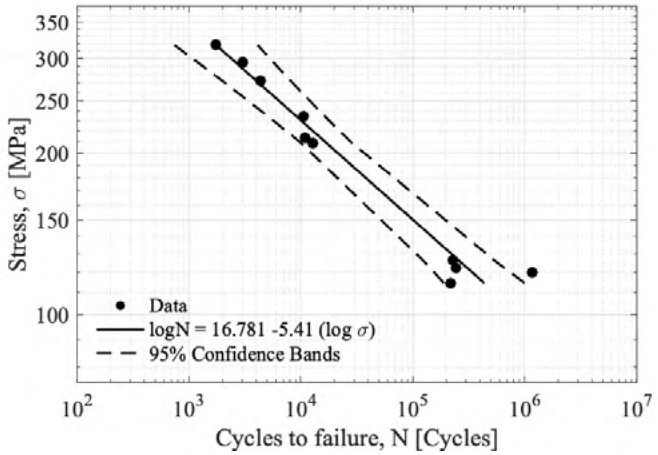

Figure 8. S-N curves of the material tests.

The fatigue tests are force controlled and are set to 30 kN, 50 kN and 70 kN. A higher force resulted in immediate failure of the ±45° plies at the outer surface. Due to large thickness differences in the specimens the forces are converted to stresses where the areas are evaluated at the location of failure, shown in Figure 9. Almost all locations of failure are concentrated in the middle region of the coupon with the narrowed cross-section according to ISO 527 – 4 to trigger the failure in this region. Due to some margins in the cutting process not all specimens had the smallest cross-section precisely in the middle, this explains why the failures don't occur precisely in the middle.

The governing failure modes occurring during the fatigue tests are delamination and/or fibre breakage respectively. This can also be seen in Figure 9. In some cases the fibre breakage progressed through the specimen in longitudinal direction towards the clamped region, while in most cases the specimen broke in the middle straight away. This progress of fibre breakage and delamination towards the clamps is better visible on the side view which is shown in Figure 9d.

Figure 9. Damage of the coupons subjected to fatigue loading of a)30kN b) 50kN c) 70kN d) Side view

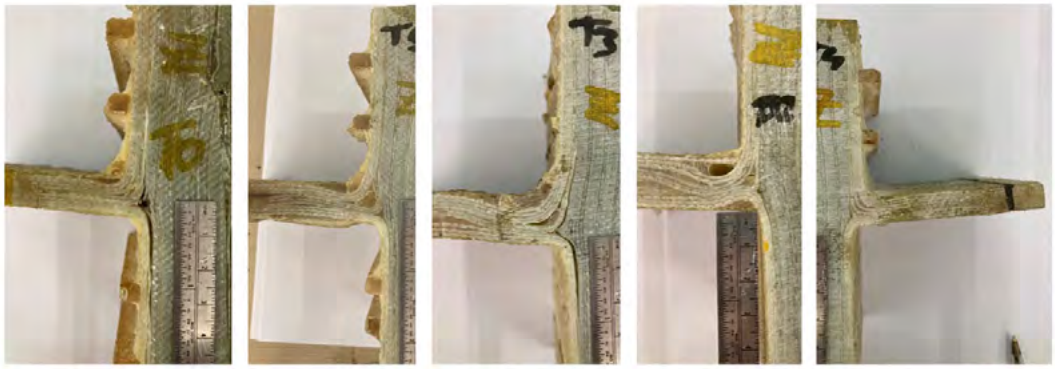

Figure 10. Failure initiation and delamination. Static component tests.

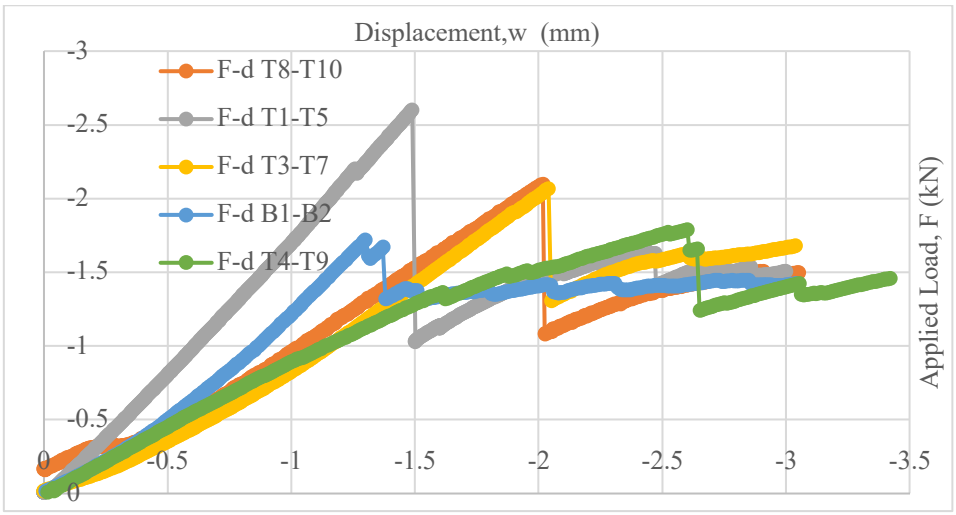

Figure 11. Load-Displacement curves. Static component tests.

3.2. Component tests

Static tests are conducted on 5 pairs of WFJ, in which one out of two connected together WFJ failed during each test. The failure modes are visually inspected, shown in Figure 10, which are similar across all the tests with the delamination between the 'Wrap' and 'UD'-layer of the WFJ. The Force-Displacement plots of the specimens are shown in Figure 11 indicating an average failure load, displacement and nominal bending stress are F_{max}=2.04kN, w_{max} = 1.90mm and σ_{max} = 50.90MPa, respectively. The nominal bending stress is determined by multiplying the reaction force from the support by the distance from the support to the beginning of the radius to obtain the bending moment. This is then divided by the elastic section modulus of the web just before the junction. All five tests show a linear relationship between the applied load and displacement.

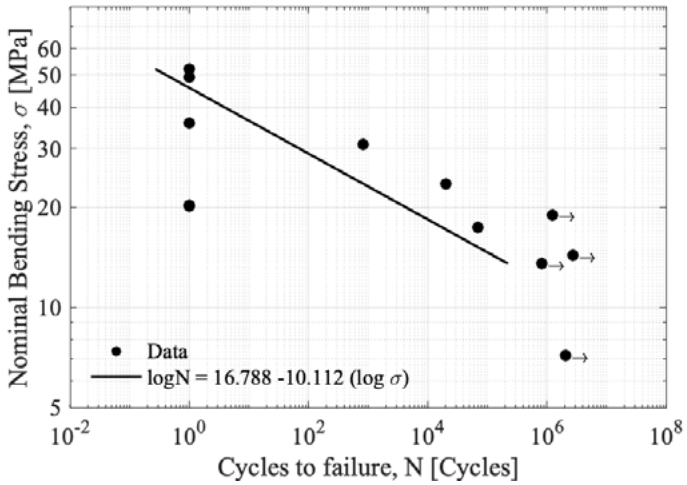

Figure 12. S-N curves of the component tests.

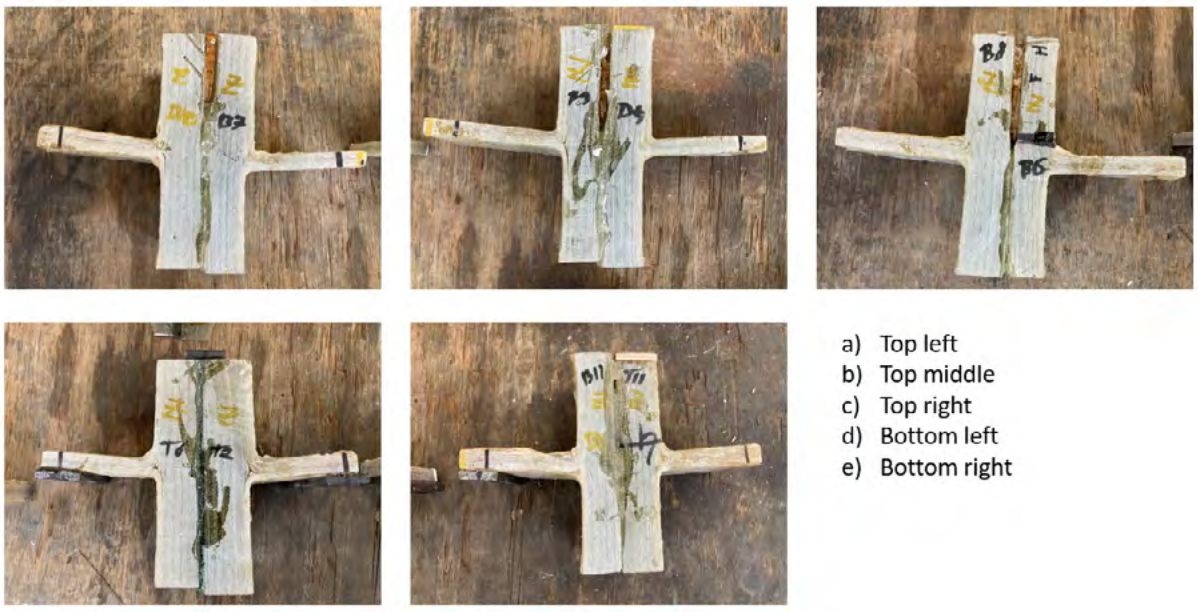

Figure 13. WFJ Component damage, fatigue tests.

The analysis of the WFJ component fatigue tests is presented in Figure 12. The tests are force-controlled with an R = 0.1. The plot includes data points along with a solid black line that represents the logarithmic

fit to the data. All the data points, except for one ($\sigma_{nom} = 7.16$MPa) are included in the fit. The equation for the fit is also shown in Figure 12.
Multiple WJF have failed at the first cycle with the applied load of 50% to 70% of ULS. Those specimens had a resin reach region in the corners of WJF, as shown in Figure 12a) and b). The specimens indicated with the arrow are stopped at around 10^6 cycles and are indicated as outruns. Similar to the static tests, the fatigue tests revealed the same failure mode: delamination between the 'wrap' and 'UD' layers, see Figure 13. The criteria for failure in the fatigue tests is determined to be crack initiation between these layers, specifically when the tangential strain in the crack direction (measured using a virtual extensometer with a 10 mm gauge length on DIC data via GOM correlate software) exceeded 0.1215% strain from the static tests. The stress correlated with the number of cycles until failure represents the nominal bending stress at the initial load cycle. Compared to the static tests, crack initiation often occurred in both junctions during the fatigue tests. This is likely due to the lower occurring stresses and longer testing times, allowing for stress redistribution and crack initiation in both junctions. However, despite quick crack initiation at low stress levels, crack growth was retarded, and no complete failure of the junction occurred in any fatigue tests.

4. Conclusions

The experimental analysis of GFRP material and WFJ components in web-core composite bridge deck panels reveals consistent failure modes across all specimens, characterized by delamination and fiber breakage during material fatigue tests, and delamination between the 'wrap' and 'UD' layers in component fatigue tests. WFJ components typically initiated fatigue under low bending stresses yet did not experience the abrupt failures with the retardation of crack propagation in between the UD layers. Although the coupon fatigue tests indicated a steep fatigue slope of 5.41, it's important to note that the material coupons tested were half the thickness of the actual deck laminate, which may influence the results' applicability to real-world scenarios.

Acknowledgments

The authors would like to express their gratitude to Rijkswaterstaat, the Directorate-General of the Ministry of Infrastructure and Water Management of the Netherlands for the financial support, and FibreCore Europe for the production of the panels.

References

[1] D. K. Rajak, D. D. Pagar, P. L. Menezes, and E. Linul, "Fiber-reinforced polymer composites: Manufacturing, properties, and applications," *Polymers*, vol. 11, no. 10. MDPI AG, Oct. 01, 2019. doi: 10.3390/polym11101667.
[2] L. C. Bank, *Composites for Construction: Structural Design with FRP Materials*. John Wiley & Sons, 2006.
[3] J. Qureshi, "Fibre-Reinforced Polymer (FRP) in Civil Engineering," in *Next Generation Fiber-Reinforced Composites - New Insights*, IntechOpen, 2023. doi: 10.5772/intechopen.107926.
[4] Technical Specification CEN/TS 19101, "Design of fibre-polymer composite structures".
[5] A. V. Movahedi-Rad, T. Keller, and A. P. Vassilopoulos, "Fatigue damage in angle-ply GFRP laminates under tension-tension fatigue," *Int J Fatigue*, vol. 109, pp. 60–69, Apr. 2018, doi: 10.1016/j.ijfatigue.2017.12.015.
[6] O. Karpenko, T. Peeters, A. Christoforidou, and M. Pavlović, "Fatigue of web-core composite bridge decks: an experimental and numerical study," Rio de Janeiro, brazil: International Conference on Fiber-Reinforced Polymer (FRP) Composites in Civil Engineering (CICE 2023), 2023. [Online]. Available: https://doi.org/10.5281/zenodo.8066285
[7] ISO 527-4: 2023, "Part 4: Test conditions for isotropic and orthotropic fibre-reinforced plastic composites."
[8] Poly Service, "POLY-POX THV 500 - HARDER 455."
[9] ASTM E739-10, "Standard Practice for Statistical Analysis of Linear or Linearized Stress-Life (S-N) and Strain-Life (ε-N) Fatigue Data."